Electronic Supplementary Information

Pendent carboxylic acid-fuelled high-performance uranium extraction in a hydrogen-bonded framework and prolifically improved water oxidation via post-metalation-actuated composite fabrication

Nilanjan Seal[a,b,*], Arun Karmakar[a,c], Subrata Kundu[a,c,*], Subhadip Neogi[a,b,*]

[a]Academy of Scientific and Innovative Research (AcSIR), Ghaziabad- 201002, India
[b]Inorganic Materials & Catalysis Division, CSIR-Central Salt & Marine Chemicals Research Institute, Bhavnagar, Gujarat 364002, India
[c]Electrochemical Process Engineering (EPE) Division, CSIR−Central Electrochemical Research Institute (CECRI), Karaikudi, Tamil Nadu 630003, India

*E-mail (Nilanjan Seal): nilanjan.seal5@gmail.com
*E-mail (Subrata Kundu): skundu@cecri.res.in and kundu.subrata@gmail.com
*E-mail (Subhadip Neogi): sneogi@csmcri.res.in and subhadip79@gmail.com

Table of contents

Section S1. Materials and Physical measurements

All the solvents and reagents were purchased from commercial sources (except H_3TCA) and used without further purification. Powder X-ray diffraction (PXRD) data were collected using a PANalytical Empyrean (PIXcel 3D detector) system equipped with Cu Kα (λ=1.54 Å) radiation. The Fourier Transform Infrared-spectra (IR) of the samples were recorded using the KBr pellet method on a Perkin–Elmer GX FTIR spectrometer in the region of 4000−400 cm^{-1}. Thermogravimetric analyses (TGA) (heating rate of 10 °C/min under N_2 atmosphere) were performed with a NETZSCH TG 209F1 Libra system. Surface area measurement was carried out using Quantachrome Autosorb IQ instrument. Scanning Electron Microscopic (SEM) and Transmission Electron Microscopic (TEM) images were obtained with a JEOL JSM 7100F and JEOL, JEM 2100 instrument, respectively. Inductively coupled plasma-mass spectrometry (ICP-MS) analysis was measured by Perkin Elmer, Optima 2000. XPS analysis was carried out using a Thermo Scientific ESCALAB 250 Xi photoelectron spectrometer (XPS) using a monochromatic Al Kα X-ray as an excitation source.

Section S2. Single Crystal X-ray Crystallography

Single crystals with suitable dimensions were chosen under an optical microscope and mounted on a glass fibre for data collection. The crystal data for **CSMCRI-21** and **CSMCRI-28** were collected on a Bruker D8 Quest diffractometer, with CMOS detector in shutter less mode. The crystals were cooled to low temperature using an Oxford Cryostream liquid nitrogen cryostat. The instrument was equipped with a graphite monochromatized MoKα X-ray source (λ = 0.71073 Å), with Triumph™ X-ray source optics. Data collection and initial indexing and cell refinement were handled using APEX II software.[1] Frame integration, including Lorentz-polarization corrections, and final cell parameter calculations were carried out using SAINT+ software.[2] The data were corrected for absorption using the SADABS program.[3] Decay of reflection intensity was monitored by analysis of redundant frames. The structure was solved using Direct methods and difference Fourier techniques. All non-hydrogen atoms were refined anisotropically. All H atoms were placed in calculated positions using idealized geometries (riding model) and assigned fixed isotropic displacement parameters. The SHELXL-2014 package within the OLEX2 crystallographic software[4] was applied for structure refinement with several full-matrix least-squares/difference Fourier cycles.[5] The disordered guest solvent molecules in the crystal lattice were treated with solvent mask option in OLEX2 software.[4] The potential solvent accessible void space was calculated using the PLATON[6] software. The crystal and refinement data for **CSMCRI-21** and **CSMCRI-28** are listed in Table S1 and S3, respectively. Topological analysis was performed by using ToposPro software.[7]

Section S3. Experimental Section

Synthesis of the ligand. The ligand, 4,4',4''-tricarboxytriphenylamine (H_3TCA) was prepared according to literature methods.[8]

Synthesis of CSMCRI-21. A mixture of $Co(NO_3)_2 \cdot 6H_2O$ (11.63 mg, 0.04 mmol), dpa (7.36 mg, 0.04 mmol) and H_3TCA (7.54 mg, 0.02 mmol) was dissolved in 1.5 mL of N,N-Dimethylformamide (DMF) and 1.5 mL of water in a 15 mL screw-capped vial. After that, it was heated to 100 °C for three days, and then slowly cooled down to room temperature. The orange colored, block shaped crystals were obtained; which were then filtered and thoroughly washed with DMF. Anal. Calcd. For $[Co_3(TCA)_3(dpa)_3] \cdot 3DMF \cdot 7H_2O$: C, 55.74; H, 4.36; N, 11.47. Found: C, 55.78; H, 4.39; N, 11.46.

Synthesis of CSMCRI-28. The synthetic procedure for **CSMCRI-28** is similar to that of **CSMCRI-21** except the fact that H_2OBA (5.16 mg, 0.02 mmol) was used instead of H_3TCA. [H_2OBA : 4,4′-Oxybis(benzoic acid)]

Synthesis of Ni^{2+}@21a. 50 mg of activated MOF and 20 mg of $NiCl_2 \cdot 6H_2O$ were taken in 20 mL of methanol. The mixture was stirred at 50 °C for 2 h, followed by filtration and thorough washing with methanol. Finally, the obtained derived material was dried at 60 °C for 4 h to get Ni^{2+}@**21a**, which was further characterized and used in performing reaction.

Preparation of working electrode using 21a and Ni^{2+}@21a. Within a mixture of 50 µL Nafion solution, 200 µL ethanol and 750 µL of distilled water, 3 mg of respective catalysts were added. After sonication for 15 min, 34.5 µL of this catalyst ink solution was drop-casted over the carbon, which was pre-treated with ethanol-acetone mixture. Hg/HgO was used as a reference electrode and carbon cloth was used as a counter electrode. The loading of each catalyst was around 0.1045 mg/cm^2.

Preparation of simulated seawater. Simulated seawater was prepared following a reported procedure.[9] 25.6 g of NaCl, 193 mg of $NaHCO_3$ and 17 mg of $UO_2(NO_3)_2 \cdot 6H_2O$ were dissolved in 1.0 L of deionized water.

Luminescence titration procedure. Finely ground **21a** (2 mg) was dispersed in 2 mL of uranyl solution with varying concentrations (3, 5, 10, 20, 50, 100, 200, 300 and 400 ppm). The mixtures were sonicated and emission spectra were collected. The probe was excited at 340 nm and emission data collection range was set from 350 to 650 nm. The regnerated MOF was collected via centrifugation, washed thoroughly with water/DCM and dried. Further characterizations and experiments were conducted using the recovered material.

Uranium adsorption kinetics experiment. To perform adsorption kinetics, 10 mg of **21a** was dipped into 10 mL of uranium nitrate solution (solid/liquid ratio = 1g/L) with uranium concentration of 10 ppm. After stirring the mixture for certain time (1, 5, 10, 20, 30, 60, 120, 180, 240, 300, 360, 480, and 600 min), the sampling solutions were centrifuged to separate the adsorbent and uranium concentration was determined by inductively coupled plasma-mass spectrometry (ICP-MS).

Uranium adsorption isotherm experiment. To perform adsorption isotherm experiments, 10 mg of **21a** was dipped into 10 mL aqueous solutions (solid/liquid ratio = 1g/L) containing different concentrations of uranium (10, 20, 50, 100, 200, 300 and 400 ppm). The mixtures were then stirred for 10 h and the resulting solutions were centrifuged to separate the adsorbent and concentrations of uranium were measured by ICP-MS.

Adsorption selectivity experiment. To investigate the adsorption selectivity of **21a** towards UO_2^{2+}, additional experiments using a series of competing metal ions (Na^+, K^+, Ca^{2+}, Ni^{2+}, Cu^{2+}, Zn^{2+}, Cd^{2+} and Sr^{2+}) (chloride salts) were carried out. In these selective adsorption experiments, concentration of all metal ions was kept 10 ppm and 10 mg of adsorbent was used at pH 5. After stirring for 10 h, the resulting solutions were centrifuged and metal ion concentrations were determined by ICP-MS.

Desorption experiment. Uranium loaded MOF (UO_2^{2+}@**21a**) was regenerated using 0.1 M Na_2CO_3 solution. The material was collected by centrifugation and washed thoroughly with deionized water followed by dichloromethane and dried. The regenerated MOF was used for next cycle of experiments and further characterization.

Uranium uptake study and related equations.

Removal percentage of UO_2^{2+}:

$$R\ (\%) = \frac{C_0 - C_t}{C_0} \times 100$$

C_0 is the initial concentration (mg/L) and C_t is the concentration at a specific time t (mg/L).

Adsorption capacity at particular time *t* (q_t) (mg/g) is defined as

$$q_t = (C_0 - C_t) \times V/m$$

V is the volume of solution (L) and *m* is the mass of adsorbent (g).

The experimental adsorption kinetic data are fitted by either pseudo-second order or pseudo-first order model, which are mentioned below:

Pseudo-first order kinetic model: $\ln(q_e - q_t) = lnq_e - k_1 t$

q_e and q_t are the amount of uranium adsorbed at equilibrium and at time t, respectively. t is the time for adsorption and k_1 is the pseudo-first order rate constant (min^{-1}).

Pseudo-second order kinetic model: $\frac{t}{q_t} = \frac{1}{k_2 q_e^2} + \frac{t}{q_e}$

k_2 is the pseudo-second order rate constant (g mg^{-1} min^{-1}).

Langmuir model of adsorption isotherm: $q_e = \frac{q_m c_e}{K_L + c_e}$

q_m is the maximum adsorption capacity (mg/g) and K_L is the Langmuir constant (L/mg).

Freundlich model of adsorption isotherm: $q_e = K_F c_e^{1/n}$

K_F is the Freundlich constant denoting adsorption capacity and n represents adsorption intensity.

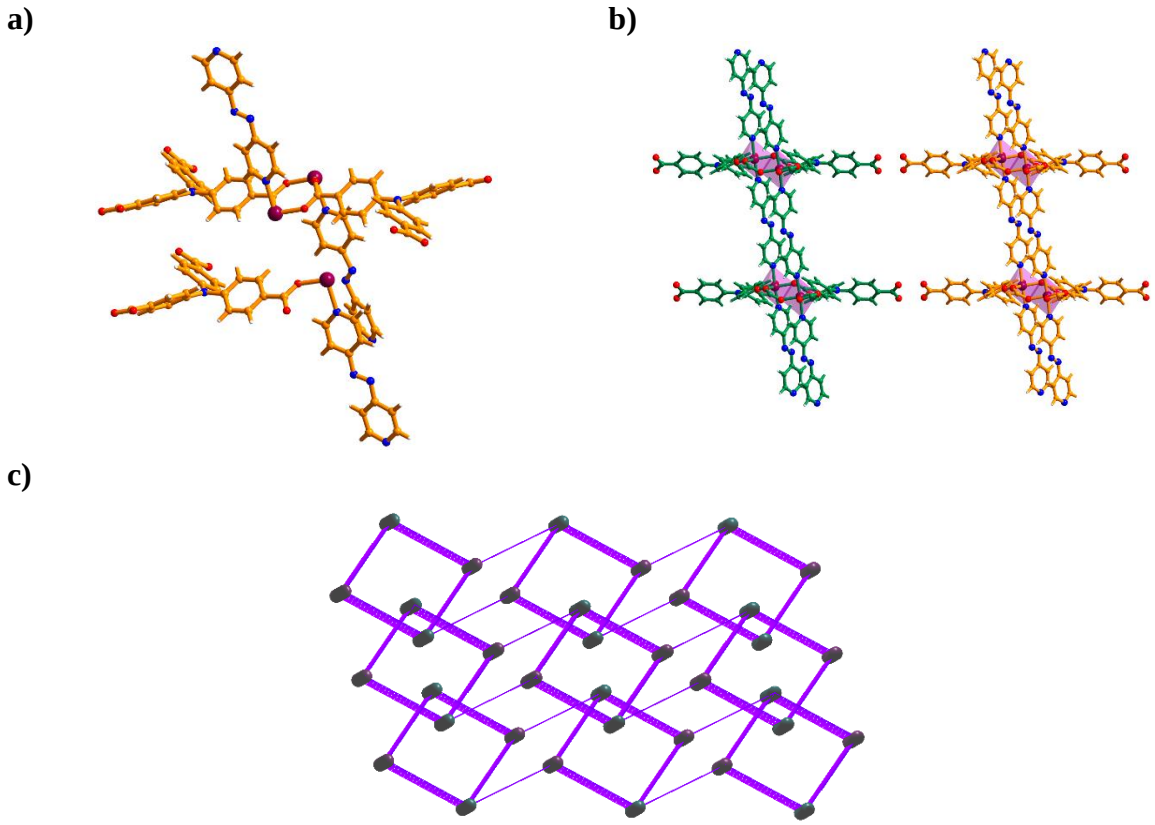

Fig. S1 (a) Asymmetric unit, (b) fish-bone shaped structure and (c) topological representation of **CSMCRI-21**.

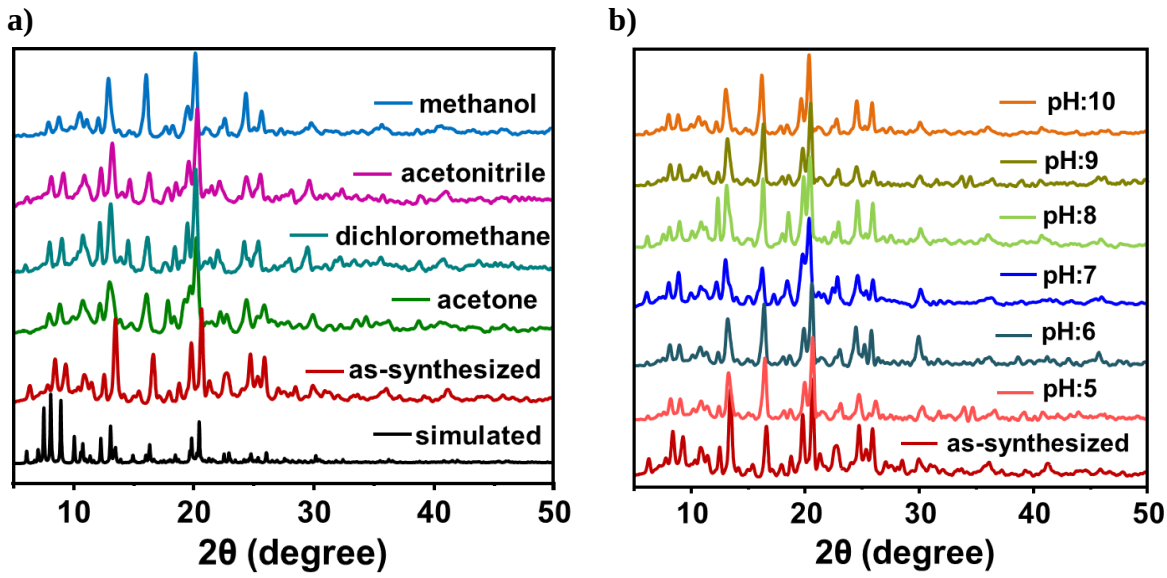

Fig. S2 PXRD pattern of the MOF (a) after immersing in some common organic solvents and (b) in diverse pH media.

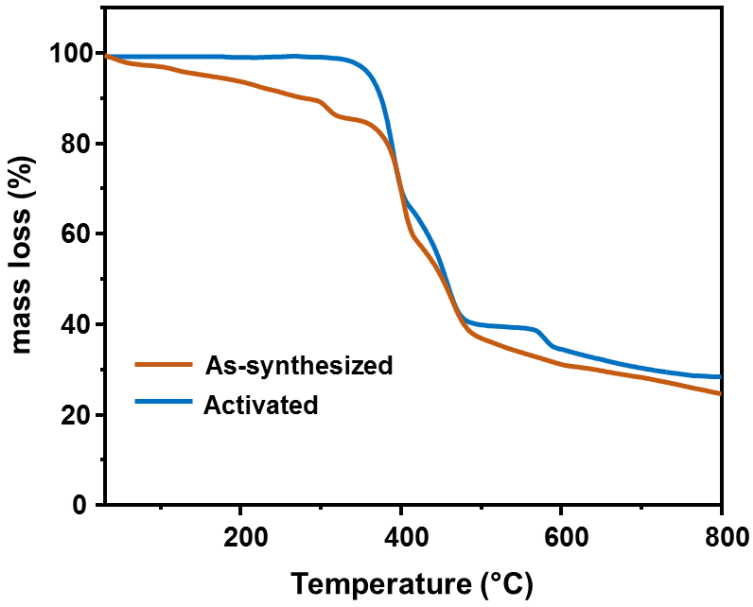

Fig. S3 Thermogravimetric analysis (TGA) of as-synthesized and activated **CSMCRI-21**.

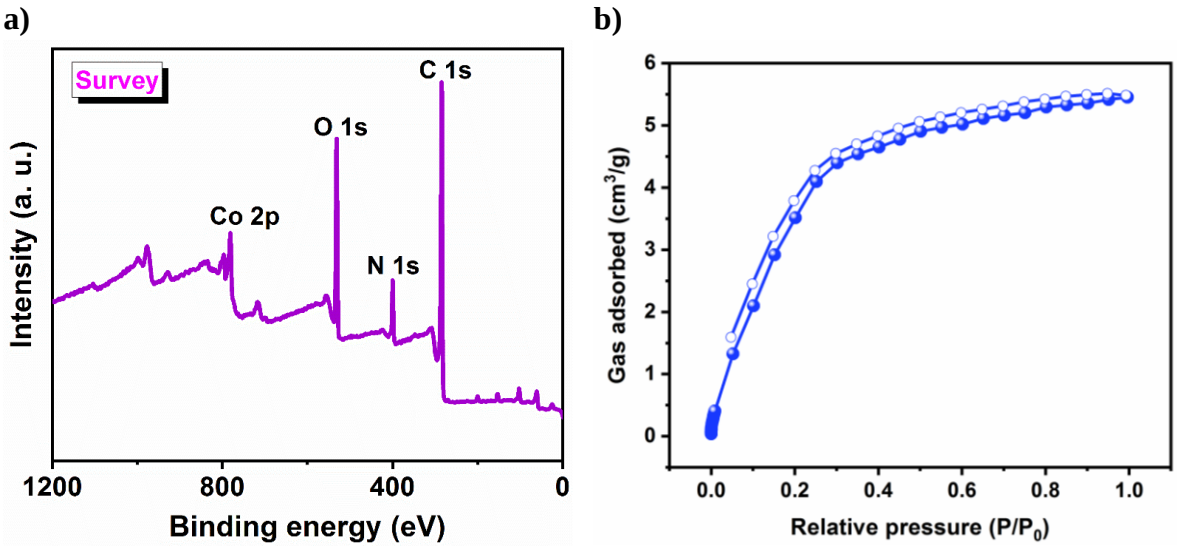

Fig. S4 (a) XPS survey spectrum of **CSMCRI-21**. (b) N_2 adsorption-desorption isotherm of activated **CSMCRI-21** at 77 K.

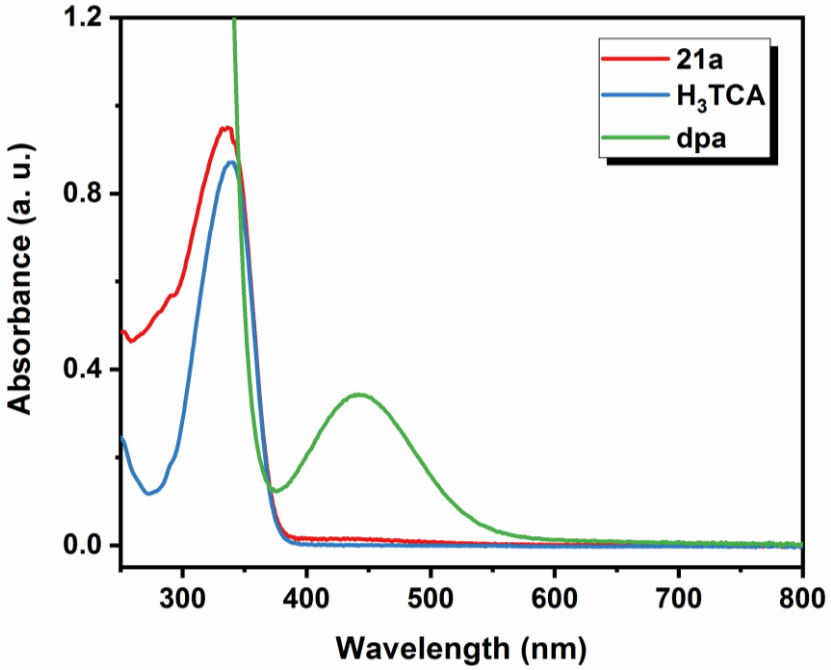

Fig. S5 UV-Vis spectra of **21a**, H_3TCA and dpa (dispersed in water).

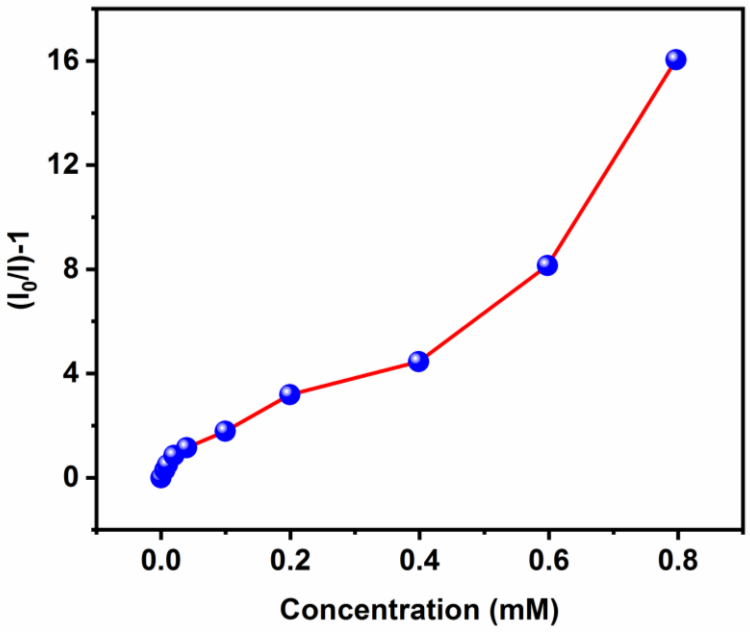

Fig. S6 The curvature of the Stern-Volmer (S–V) plot for UO_2^{2+} sensing.

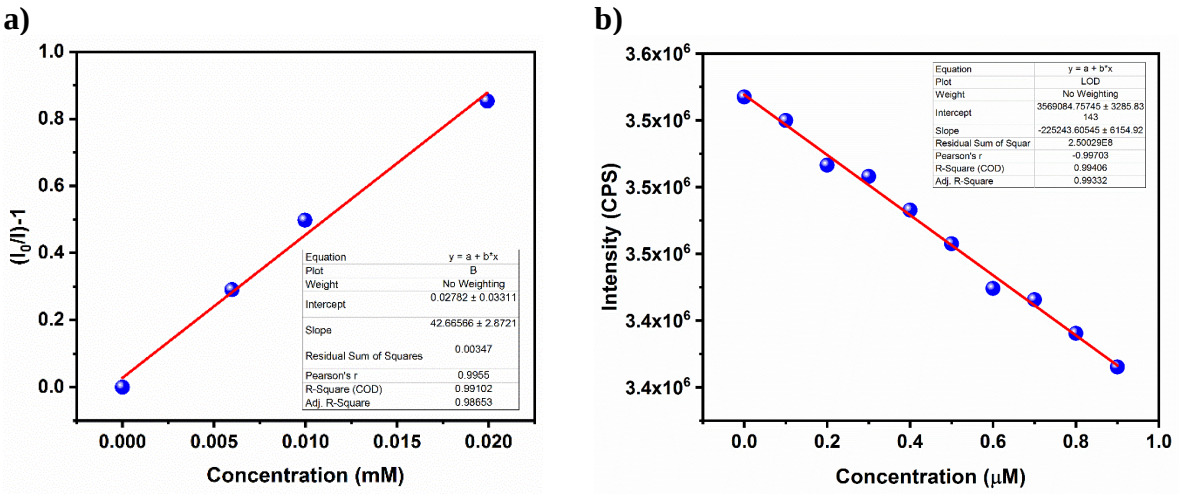

Fig. S7 (a) Linear region of Stern-Volmer (S-V) plot for UO_2^{2+} sensing. (b) Linear region of fluorescence intensity of **21a** upon addition of 10 μM UO_2^{2+} solution.

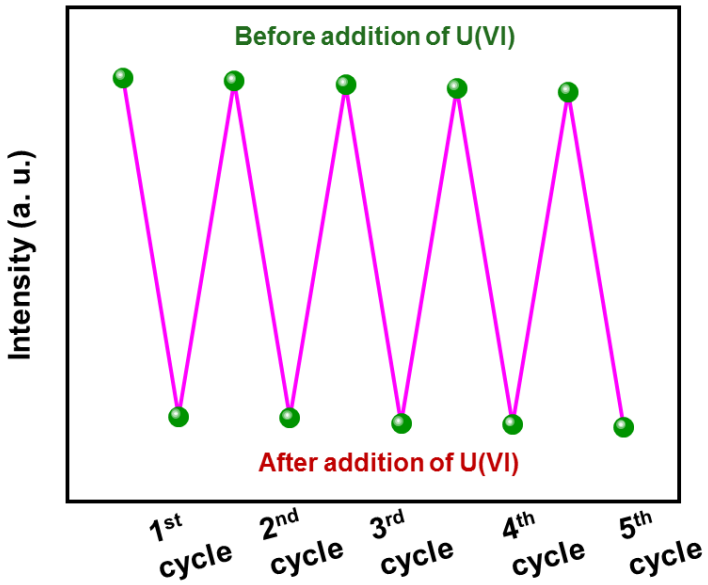

Fig. S8 Reproducibility of quenching efficiency of **21a** towards U(VI) up to five sensing recovery cycles.

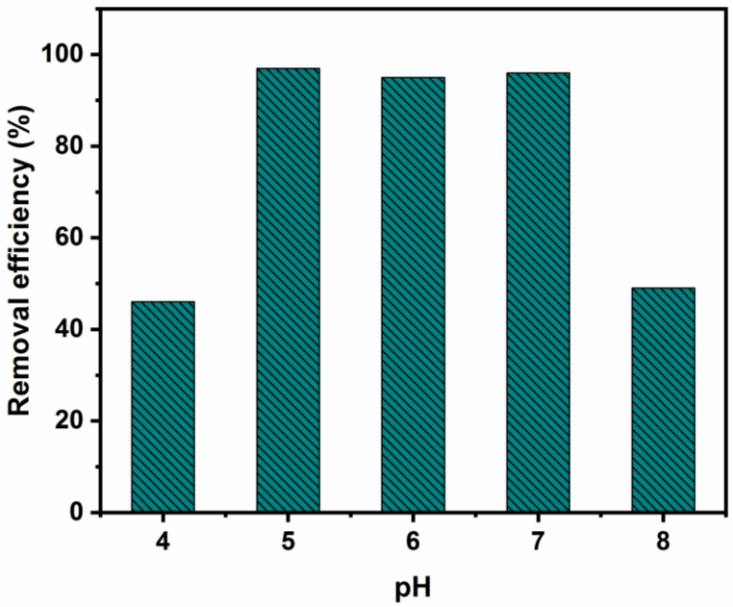

Fig. S9 pH dependency of U(VI) uptake by **21a**.

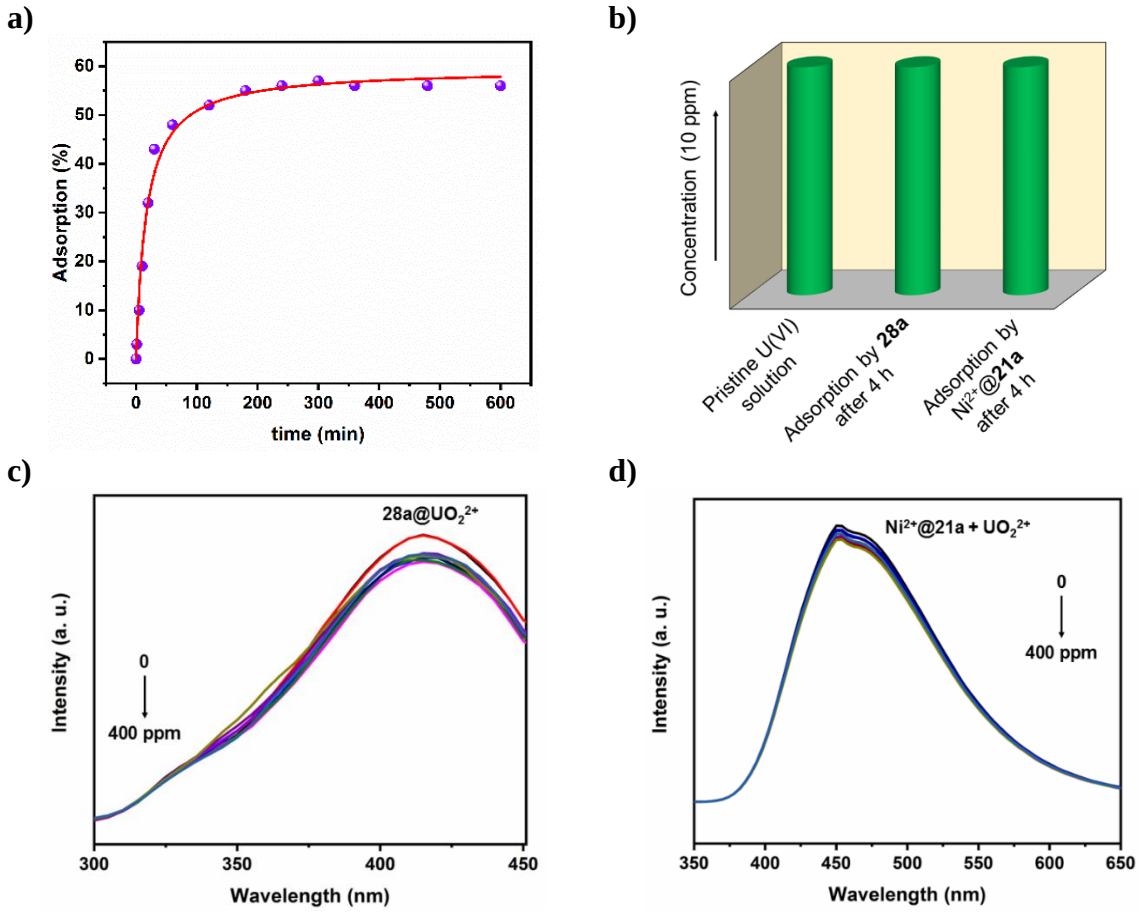

Fig. S10 (a) Uranyl adsorption by **21a** from simulated seawater. (b) U(VI) adsorption by **28a** and Ni^{2+}@**21a**. Emission spectra of (c) **28a** and (d) Ni^{2+}@**21a** upon addition of U(VI) solution.

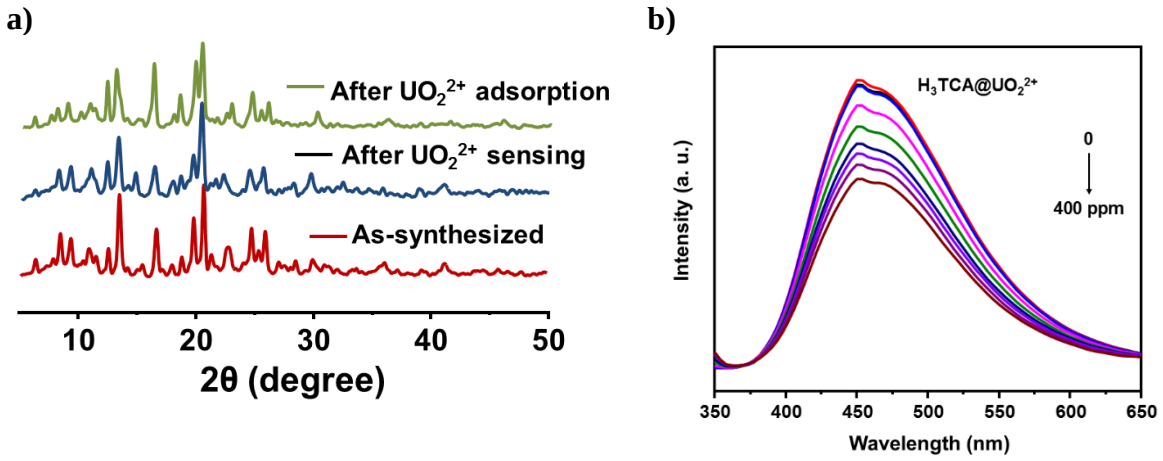

Fig. S11 (a) PXRD pattern of the MOF after sensing and adsorption of U(VI). (b) PL quenching of H_3TCA in presence of U(VI).

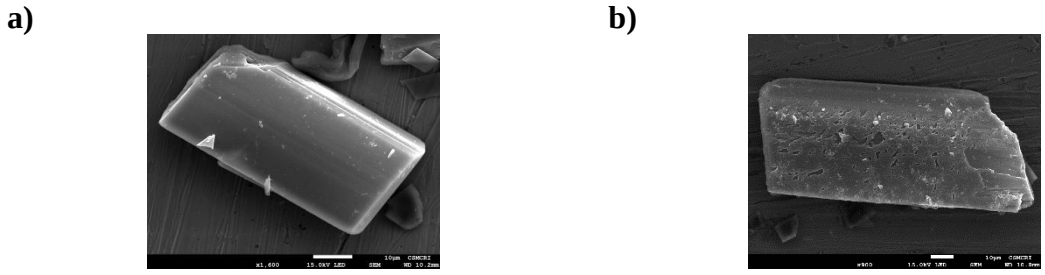

Fig. S12 FE-SEM images of (a) **CSMCRI-21** and (b) after U(VI) sensing.

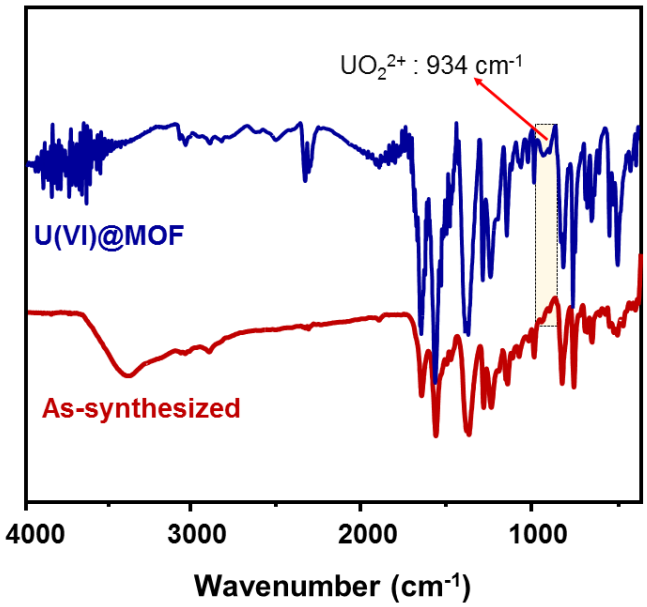

Fig. S13 FT-IR spectra of the MOF before and after adsorption of U(VI).

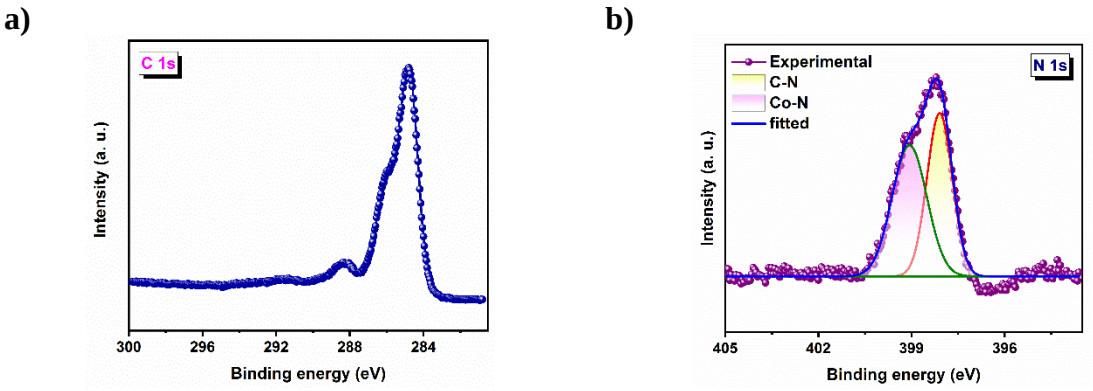

Fig. S14 High-resolution XPS spectrum of (a) C 1s and (b) N 1s of UO_2^{2+}@**21a**.

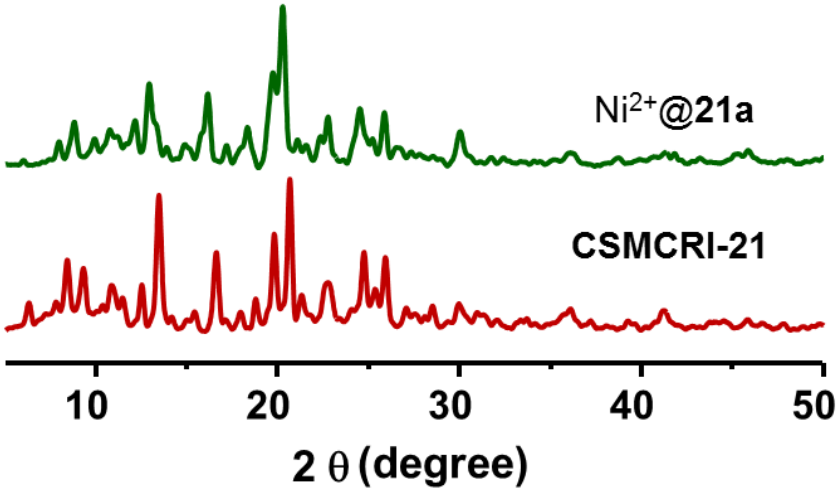

Fig. S15 PXRD patterns of Ni^{2+}@**21a** and as-synthesized **CSMCRI-21**.

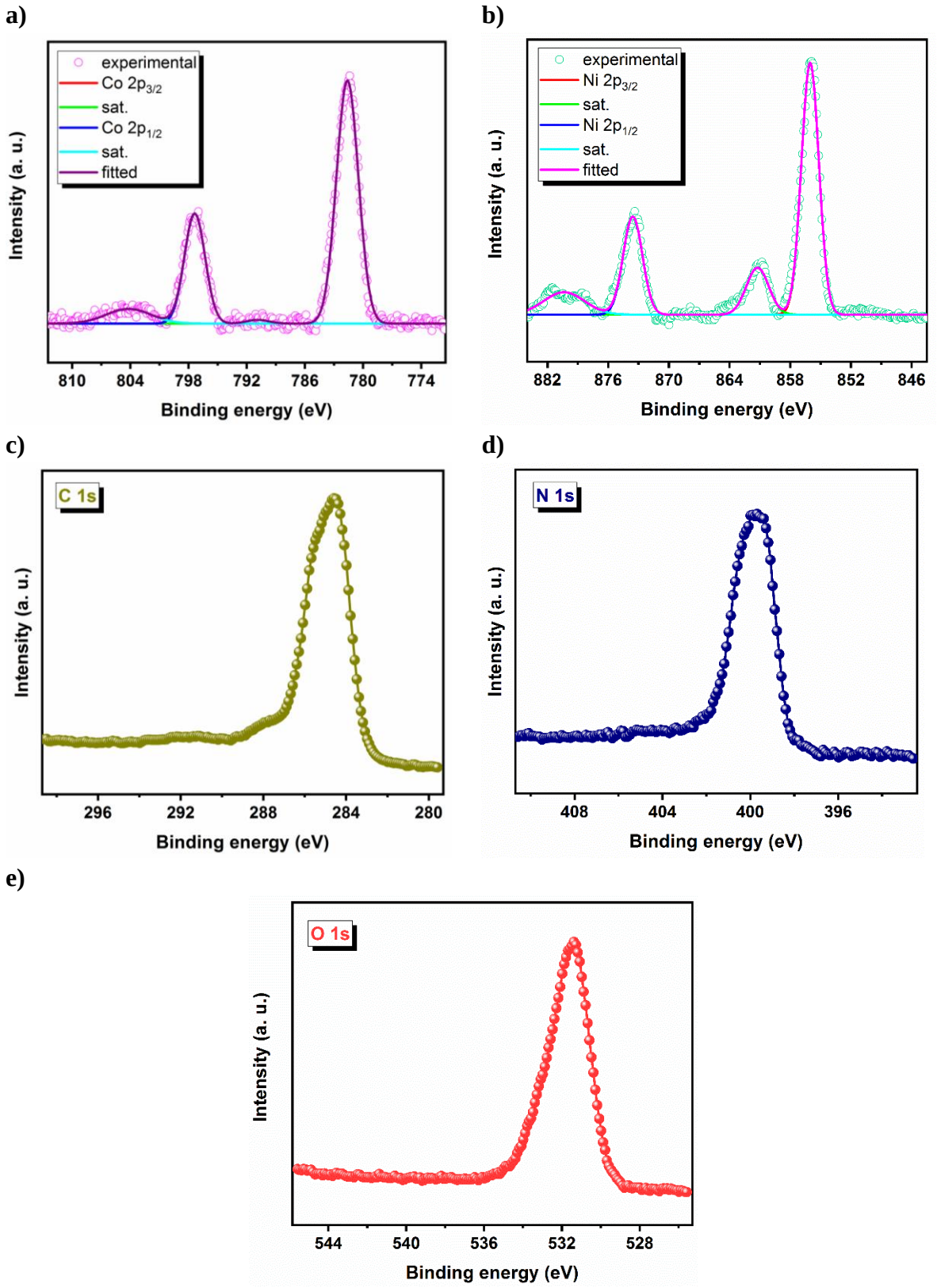

Fig. S16 High-resolution XPS spectra of Ni^{2+}@**21a** consisting of (a) Co 2p, (b) Ni 2p, (c) C 1s, (d) N 1s and (e) O 1s.

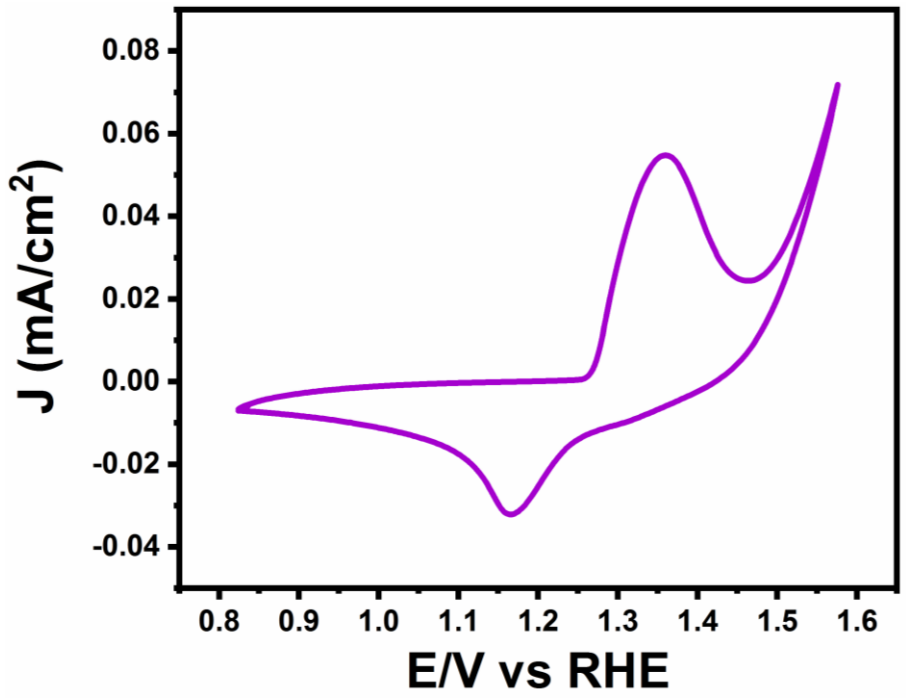

Fig. S17 Cyclic voltammetry of **21a** revealing the oxidation process of Co^{2+} to Co^{3+}.

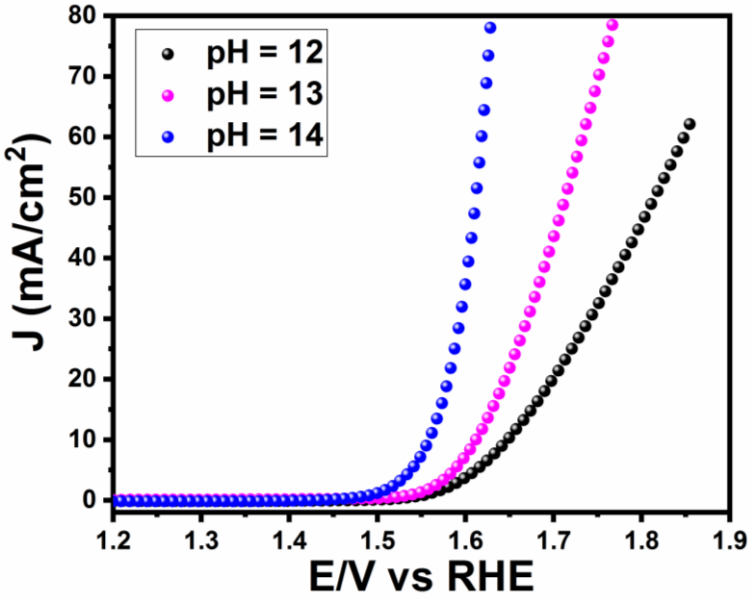

Fig. S18 pH dependent LSV measurement for Ni^{2+}@**21a**.

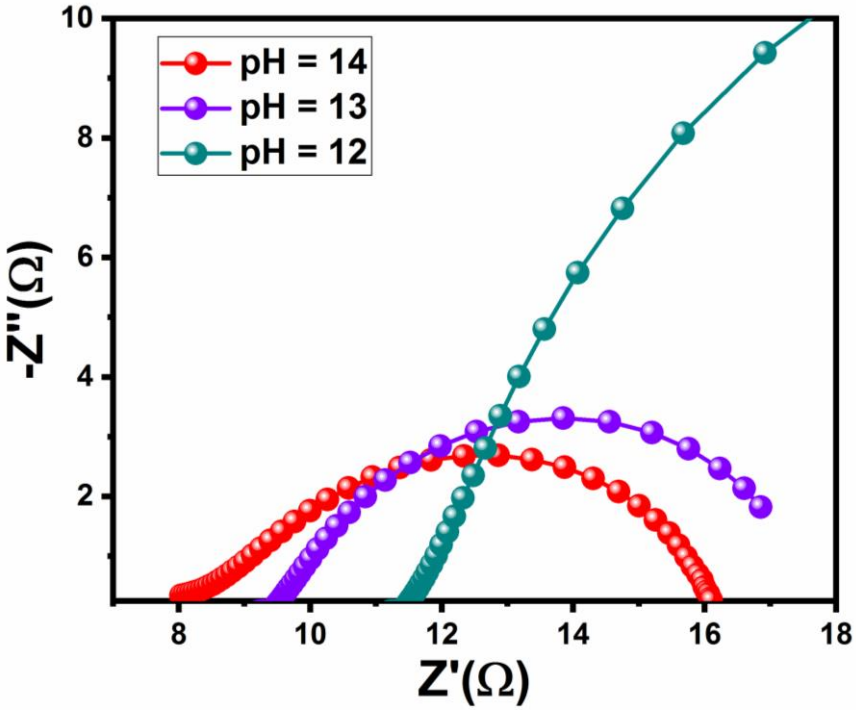

Fig. S19 pH dependent electrochemical impedance spectroscopic measurement for **21a**.

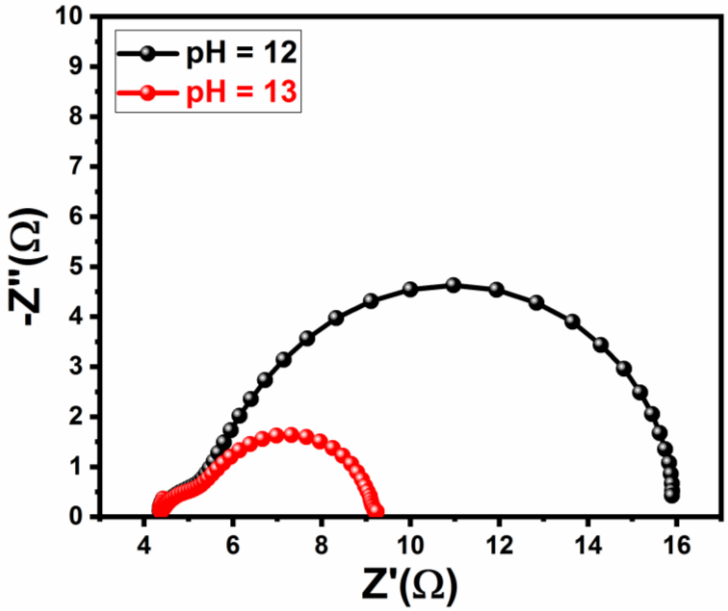

Fig. S20 pH dependent electrochemical impedance spectroscopic measurement for Ni^{2+}@**21a**.

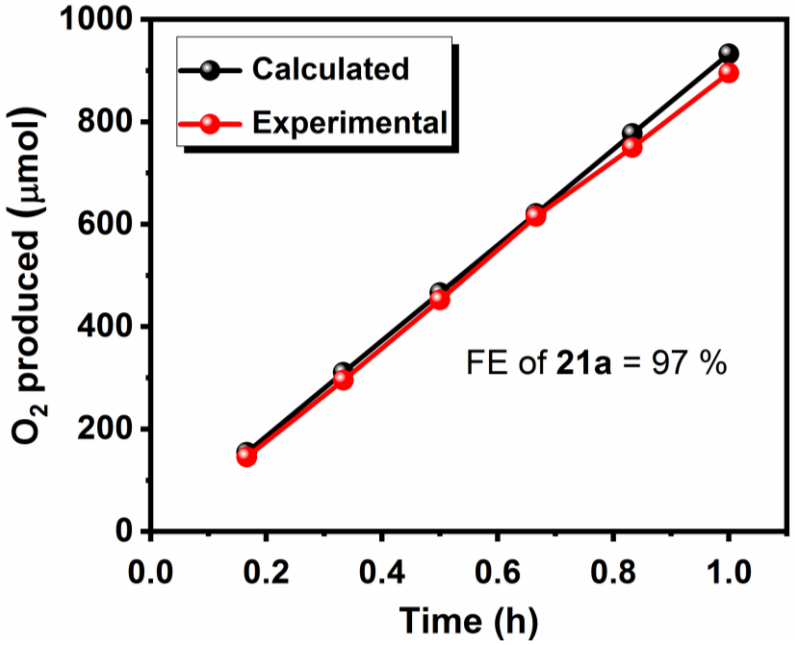

Fig. S21 Theoretical and experimental amounts of oxygen evolution for **21a** during OER electrocatalysis.

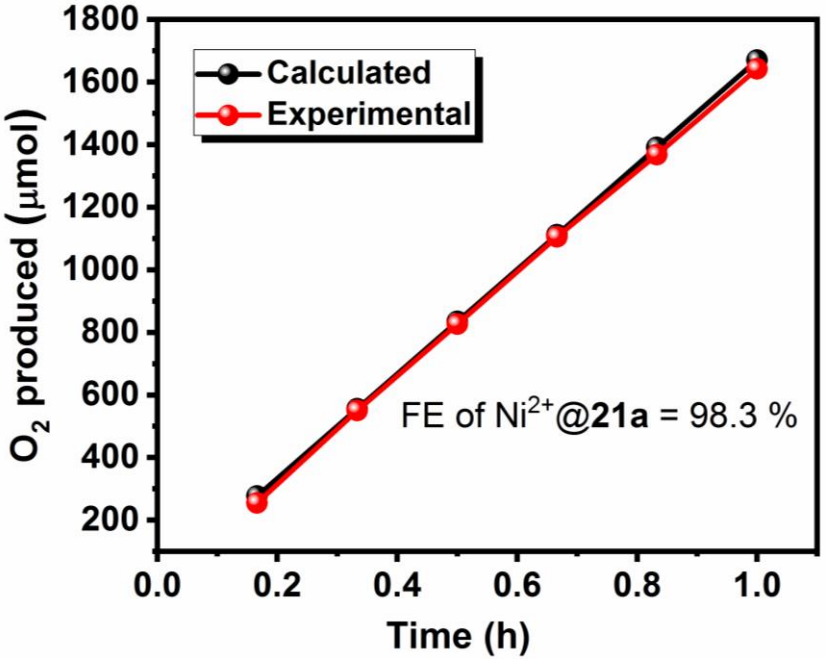

Fig. S22 Theoretical and experimental amounts of oxygen evolution for Ni^{2+}**21a** during OER electrocatalysis.

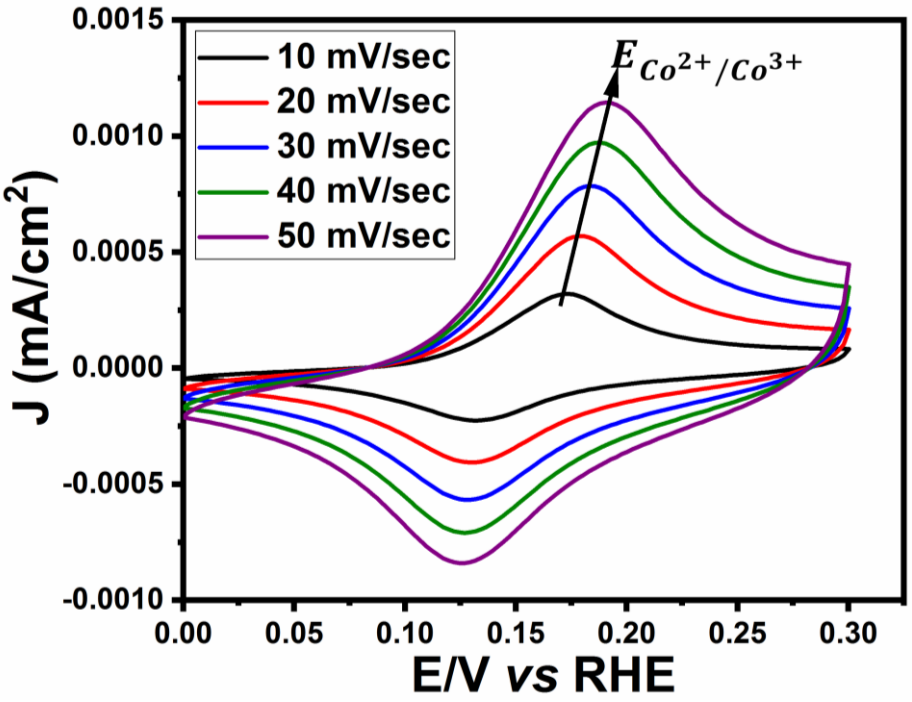

Fig. S23 Cyclic voltammetry plot for **21a** at various scan rates (50 mV/s to 10 mV/s) in the non-Faradaic region.

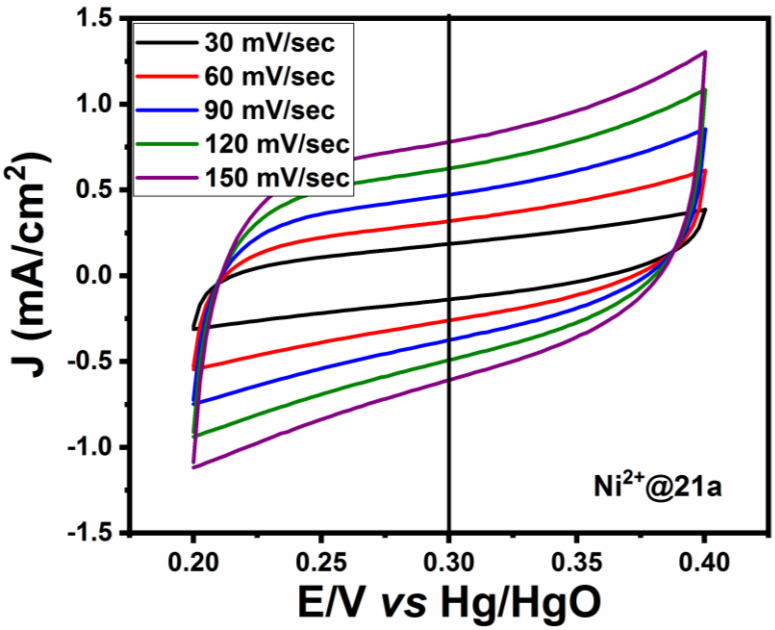

Fig. S24 Cyclic voltammetry plot for Ni^{2+}@**21a** at various scan rates (150 mV/s to 30 mV/s) in the non-Faradaic region.

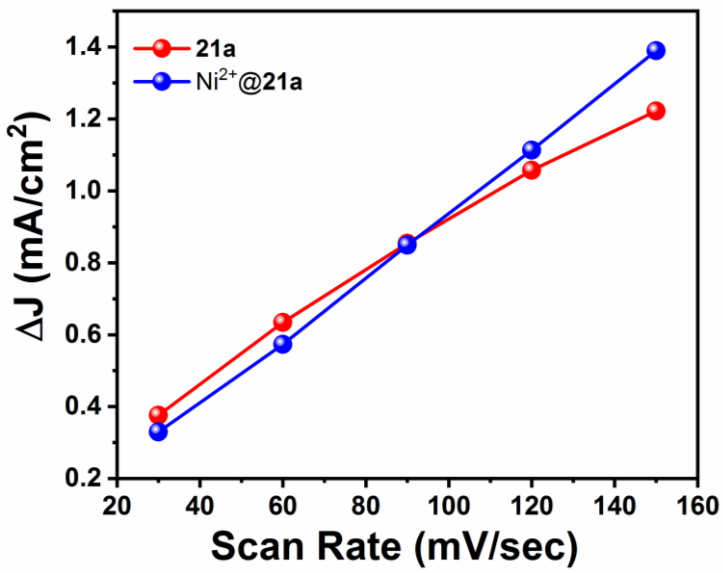

Fig. S25 Plot of capacitive current as a function of scan rate for **21a** and commercial NiO in the non-Faradaic region.

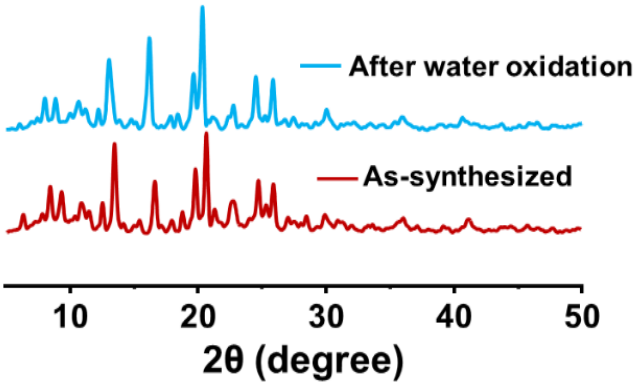

Fig. S26 PXRD pattern of the MOF after water oxidation.

a) **b)**

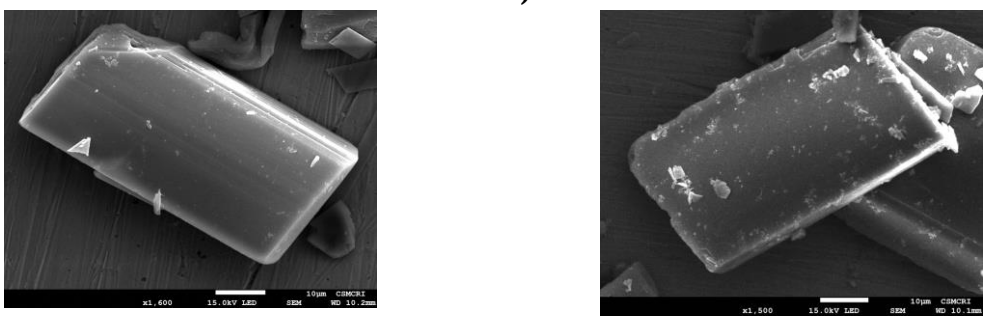

Fig. S27 FE-SEM images of the MOF before (a) and after (b) water oxidation.

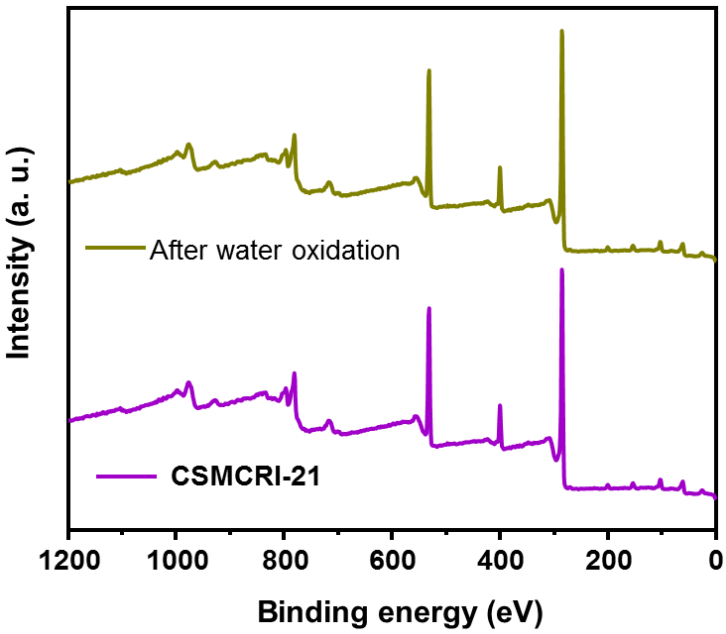

Fig. S28 XPS survey spectrum of the MOF after water oxidation.

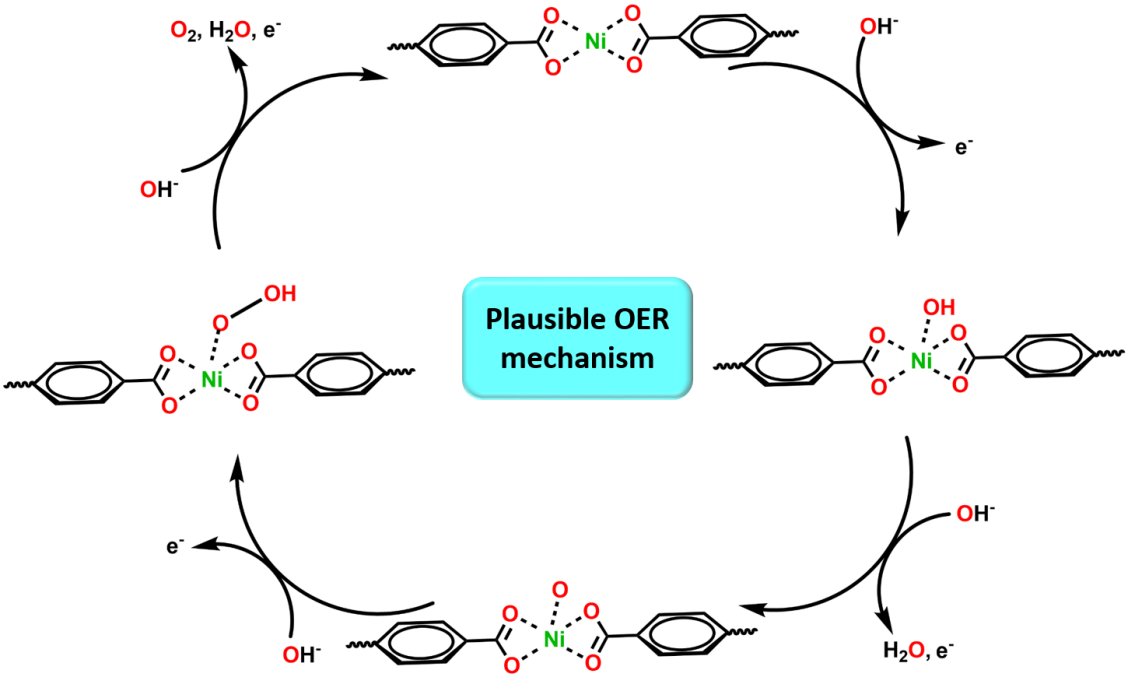

Fig. S29 Proposed mechanism for Ni^{2+}@**21a**-catalyzed OER.

Table S1. Crystal data and refinement parameters for **CSMCRI-21**

Identification code	**CSMCRI-21**
Empirical formula	$C_{93}H_{60}Co_3N_{15}O_{18}$
Formula weight	1852.40
Temperature/K	302.15
Crystal system	triclinic
Space group	*P*-1
a/Å	13.3607(9)
b/Å	14.7831(9)
c/Å	25.4340(18)
α/°	97.603(2)
β/°	97.392(2)
γ/°	100.151(2)
Volume/Å^3	4841.6(6)
Z	2
ρ_{calc}g/cm^3	1.2705
μ/mm^{-1}	0.579
F(000)	1899.0
Crystal size/mm^3	0.467 × 0.19 × 0.08
Radiation	Mo Kα (λ = 0.71073)
2Θ range for data collection/°	4.58 to 56.74
Index ranges	-17 ≤ h ≤ 17, -19 ≤ k ≤ 19, -33 ≤ l ≤ 33
Reflections collected	137213
Independent reflections	24065 [R_{int} = 0.0819, R_{sigma} = 0.0691]
Data/restraints/parameters	24065/0/1163
Goodness-of-fit on F^2	1.081
Final R indexes [I>=2σ (I)]	R_1 = 0.0599, wR_2 = 0.1604
Final R indexes [all data]	R_1 = 0.1117, wR_2 = 0.2009
Largest diff. peak/hole / e Å^{-3}	2.63/-0.90

Determination of formula & solvent composition of CSMCRI-21 from PLATON Squeezeand Thermogravimetric analysis data:

From the TGA plot of as-synthesized **CSMCRI-21**, the observed mass loss is 15.19 %

From PLATON Squeeze program void electron count / unit cell comes out to be 190.5

As DMF and water were used as solvents during the synthesis of the MOF, so the void space should be occupied by these lattice solvent molecules.

Now, formula of the asymmetric unit excluding guest solvents is $[Co_3(TCA)_3(dpa)_3]$, and mass of this asymmetric unit is 1854.4

Table S2. Number of electrons and molecular mass of guest molecules associated with **CSMCRI-21** for determination of solvent composition and molecular formula

	Dimethyl formamide (DMF)	Water
No. of electrons	40	10
mass	73	18

Considering the above mentioned number of electrons, the best possible combination of solvent molecules for **CSMCRI-21** could be $[Co_3(TCA)_3(dpa)_3]\cdot 3DMF\cdot 7H_2O$

The total number of electrons contributed by lattice solvent molecules will be [(40×3) + (10×7)] = 190, which is in complete agreement with the PLATON result and thus validates the above formula.

The aforementioned combination was further cross-checked from TGA analysis.

Mass loss due to lattice solvents is [(73×3) + (18×7)] = 345

Therefore, total mass of **CSMCRI-21** including lattice solvents is (1854.4+345) = 2199.4

So mass loss due to lattice water molecules is [(126/2199.4) ×100] % = 5.72 %

Mass loss due to lattice DMF molecules is [(219/2199.4) ×100] % = 9.95 %

So total mass loss for solvents is (5.72+9.95) % = 15.67 %, which is in good agreement with that of the TGA result.

Table S3. Crystal data and refinement parameters for **CSMCRI-28**

Identification code	**CSMCRI-28**
Empirical formula	$C_{24}H_{16}CoN_4O_5$
Formula weight	499.35
Temperature/K	273.15
Crystal system	triclinic
Space group	P-1
a/Å	9.081(4)
b/Å	11.007(6)
c/Å	14.835(7)
α/°	70.42(2)
β/°	84.50(2)
γ/°	82.93(2)
Volume/Å^3	1384.1(12)
Z	2
ρ_{calc}g/cm^3	1.1980
μ/mm^{-1}	0.656
F(000)	510.9
Radiation	Mo Kα (λ = 0.71073)
2Θ range for data collection/°	3.94 to 61.46

Index ranges	$-12 \leq h \leq 13$, $-15 \leq k \leq 15$, $-21 \leq l \leq 21$
Reflections collected	94181
Independent reflections	8570 [R_{int} = 0.0804, R_{sigma} = 0.0382]
Data/restraints/parameters	8570/0/307
Goodness-of-fit on F^2	1.087
Final R indexes [I>=2σ (I)]	R_1 = 0.0413, wR_2 = 0.1278
Final R indexes [all data]	R_1 = 0.0603, wR_2 = 0.1509

Table S4. A comparison of quenching constant, their LOD values, of various luminescent MOFs used for detection of uranyl ion

Entry	LMOF/Coordination polymer	Quenching constant (M^{-1})	Limit of Detection (LOD)	References
1.	YTU-100	8.1×10^4	1.07 ppb	*ACS Appl. Mater. Interfaces* **2021**, *13*, 51086−51094
2.	ECUT-135	-	5.4 ppb	*J. Solid State Chem.* **2021**, *299*, 122153
3.	$(CH_3)_2NH_2[Eu_2(BTC)(AC)_3(FM)]$	8.56×10^3	4.12 µM	*J. Mol. Struct.* **2021**, *1238*, 130422-130431
4.	$[Gd_2(adip)(H_2adip)(NMP)_2]\cdot DMF\cdot 3H_2O$	4.05×10^4	1.42 µM	*Inorg. Chem.* **2020**, *59*, 18027−18034
5.	HNU-50	-	0.012 µM	*Inorg. Chem.* **2020**, *59*, 9857−9865
6.	LnCPs	6.19×10^4	1.95 µM	*J. Chem. Res.* **2020**, *45*, 130-135
7.	$[Eu_2(MTBC)(OH)_2(DMF)_3(H_2O)_4]\cdot 2DMF\cdot 7H_2O$	3.6315×10^3	309.2 µg/L	*Talanta* **2019**, *196*, 515–522
8.	$[Eu_2(TATAB)_2]\cdot 4H_2O\cdot 6DMF$	4.8×10^4	0.9 µM	*Anal. Bioanal. Chem.* **2019**, *411*, 4213-4220
9.	$[Tb_2(TATAB)_2]\cdot 4H_2O\cdot 6DMF$	-	0.9 µg/L	*Environ. Sci. Technol.* **2017**, *51*, 3911−3921
10.	[Co(dmimpym)(nda)$_2$]n	1.1×10^4	13.2 µM	*J. Mater. Chem. A* **2017**, *5*, 13079–13085
11.	$[In_2(OH)_2(H_2TTHA)(H_2O)_2]_n$	4.8×10^4	0.42 ppm	*ACS Appl. Mater. Interfaces* **2016**, *8*, 28718−28726
12.	**CSMCRI-21**	4.26×10^4	0.13 µM/ 0.24 ppm	**This work**

Table S5. A comparison of uptake capacities for uranium (VI) by diverse adsorbents

Entry	Adsorbent	pH	Adsorption capacity (mg/g)	References
1.	i-MZIF90(50)	7	1489.13	*Energy Environ. Sci.* **2022**, 15, 3462–3469
2.	YTU-100	-	83.43	*ACS Appl. Mater. Interfaces* **2021**, 13, 51086−51094

3.	HNU-50	3	632	*Inorg. Chem.* **2020**, 59, 9857−9865
4.	UCY-13	3	984	*J. Mater. Chem. A* **2020**, 8, 1849
5.	USC-CP-1	5.5	562	*Angew. Chem. Int. Ed.* **2019**, 58, 18808
6.	SCU-19	4	557	*Angew. Chem. Int. Ed.* **2019**, 58, 16110 –16114
7.	JXNU-4	4	129	*Eur. J. Inorg. Chem.* **2019**, 735–739
8.	ECUT-100	5	381	*J. Solid State Chem.* **2018**, 266, 244-249
9.	Azo-MOF	5	200	*J. Solid State Chem.* **2018**, 265, 148-154
10.	MOF-5	5	237	*Sci. Bull.* **2018**, 63, 831-839
11.	ZIF-67	4	1683.8	*Colloids Surf. A: Physicochem. Eng.* **2018**, 547, 73−80
12.	Co-SLUG-35	9	119	*Chem. Eng. J.* **2017**, 316, 154–159
13.	$[Tb_2(TATAB)_2]\cdot 4H_2O\cdot 6$ DMF	4	179.08	*Environ. Sci. Technol.* **2017**, *51*, 3911−3921
14.	ZS-2	4.5	58	*Nat. Commun.* **2017**, 8, 15369
15.	MIL-101(Cr)-traiziole-COOH	7	314	*ACS Appl. Mater. Interfaces* **2016**, 8, 31032
16.	$Zn(ADC)(4,4'\text{-}BPE)_{0.5}$	6	312.32	*J. Radioanal. Nucl. Chem.* **2016**, 310, 353−362
17.	$Zn(HBTC)(L)\cdot(H_2O)_2$	2	125	*J. Mater. Chem. A* **2015**, 3, 13724–13730
18.	MOF-76	3	298	*Chem. Commun.* **2013**, 49, 10415
19.	HKUST-1	6	787.4	*Colloids Surf. A: Physicochem. Eng.* **2013**, 431, 87−92
20.	**CSMCRI-21**	5	129.8	**This work**

Table S6. The distribution coefficient (K_d) values calculated for 10 ppm solutions of diverse cations at V/m = 1000 mL g^{-1}

Ions	**Distribution coefficient (K_d) ($\times 10^3$) (mL g^{-1})**	**Selectivity**
UO_2^{2+}	49	-
Cu^{2+}	0.81	60.4
Ni^{2+}	0.85	57.6
Zn^{2+}	0.72	68

Cd^{2+}	0.61	80.3
Ca^{2+}	0.63	77.7
Sr^{2+}	0.42	116.6
Na^{+}	0.11	445.4
K^{+}	0.13	376.9

Table S7. A comparison of electrocatalytic performance of activated **CSMCRI-21** and Ni^{2+}@**21a** in water oxidation to that of contemporary materials

Entry	Material	Over-potential (mV)	Tafel slope (mV/dec)	TOF (s^{-1})	Reference
1.	Ek-a	413 (pH 14.0)	77	0.004	*J. Mater. Chem. A*, **2021**, *9*, 26800-26809
2.	NiPc–Ni	427 (pH 14.0)	83	11.32	*J. Mater. Chem. A*, **2021**, *9*, 1623-1629
3.	Ni-MOF/LDH	220	36	-	*Appl. Catal. B* **2021**, 286, 119906
4.	NiFe-HXR	289	43	4.54	*ChemSusChem* **2021**, *14*, 1830–1834
5.	Ni-MOF/NF	350	98	0.24	*Inorg. Chem. Front.* **2021**, *8*, 3007-3011
6.	NiFe LDH@$FeNi_3$	380 (pH 14.0)	172	-	*J. Mater. Chem. A*, **2022**, *10*, 5442-5451
7.	Ni-MOF/NF	362	98	0.024	*Inorg. Chem.* **2020**, *59*, 4764 − 4771
8.	Wire-like MoS_2/r$FeNiCo_2O_4$	270	39	-	*J. Am. Chem. Soc.* **2020**, *142*, 50–54
9.	SCF-800	327	62	-	*J. Mater. Chem. A* **2020**, *8*, 6480-6486
10.	M-PCBN	232	32	-	*ACS Nano* **2020**, *14*, 1971–1981
11.	$Co_3(HITP)_2$	254 (pH 14.0)	86.5	-	*Appl. Catal. B*, **2020**, *278*, 119295.
12.	$Fe_{0.38}Ni_{0.62}$-MOF	190	58.3	3.65	*ACS Appl. Nano Mater.* **2019**, *2*, 6334 − 6342
13.	Fe_2O_3@Ni-MOF-74	264	48	12.4×10^{-2}	*Inorg. Chem.* **2019**, *58*, 11500 − 11507
14.	Co_2-MOF@Nafion	537@5 mA/cm^2 (pH 7.0)	105±5	0.026	*ACS Appl. Mater. Interfaces* **2019**, *11*, 46658−46665
15.	Ni-MOF/NF	320	123	0.25	*Inorg. Chem. Front.* **2018**, *5*, 1570-1574
16.	Fe/$Ni_{2.4}$/$Co_{0.4}$-MIL-53	236	52.2	-	*Angew. Chem. Int. Ed.* **2018**, *57*, 1888-1892
17.	Ni-MOF@Fe-MOF	265	82	-	*Adv. Funct. Mater.* **2018**, *28*, 1801554- 1801563

18.	Co:Fe_3	453	63	0.088	*J. Am. Chem. Soc.* ***2017****, 139, 5*, 1778–1781
19.	ALD NiS_x	372	56	-	*Chem. Mater.* **2016**, *28*, 1155–1164
20.	Co-TpBpy	400	59	0.23	*Chem. Mater.* **2016**, *28*, 4375-4379
21.	CoNi SUNOE	450	38.5	-	*Chem. Sci.* **2015**, *6*, 3572–3576
22.	NG-$CoSe_2$	366	40	0.03	*ACS Nano* **2014**, *8*, 3970-3978
23.	Co-ZIF-9	510	193	1.76×10^{-3}	*Nanoscale* **2014**, *6*, 9930-9934
24.	CSMCRI-10	396 (pH 14.0)	102	0.03	*Chem. Eng. J.* **2022**, *429*, 132301
25.	MOF-2	370	101.9	0.6	*ACS Appl. Mater. Interfaces* **2020**, *12*, 33679−33689
26.	NH_2TA-Ni-MOF	356	105	1.26×10^{-2}	*Chem. Eur. J.* **2019**, *25*, 11141 – 11146
27.	CoCd-MOF	353	110	3.314×10^{-2}	*ACS Appl. Mater. Interfaces* **2017**, *9*, 37548−37553
28.	Co-WOC-1	390	128	0.05	*Angew. Chem., Int. Ed.* **2016**, *55*, 2425-2430
29.	UTSA-16	408	77	-	*ACS Appl. Mater. Interfaces* **2017**, *9*, 7193−7201
30.	**CSMCRI-21** Ni^{2+}@**21a**	331 308	62 38	3.45 12.7	**This work**

CheckCIF alert explanations

For **CSMCRI-21**

PLAT910_ALERT_3_B Missing # of FCF Reflection(s) Below Theta(Min). 13 Note

Explanation: This alert was generated due to omission of some reflections in the refinement process for technical reasons.[10]

For **CSMCRI-28**

PLAT919_ALERT_3_B Reflection # Likely Affected by the Beamstop ... 2 Check

Explanation: This alert is due to large unit-cell causing reflections affected by the beamstop, which could not be rectified due to low-grade crystal quality.[11]

PLAT934_ALERT_3_B Number of (Iobs-Icalc)/Sigma(W) > 10 Outliers .. 5 Check

Explanation: This alert is due to a consequence of low-grade data quality.[10,12]

References

1) *APEX2*, v. 2014.7-1; Bruker AXS: Madison, WI, 2014.
2) *SAINT*, v. 8.34A; Bruker AXS: Madison, WI, 2013.
3) *SADABS*, v. 2014/3; Bruker AXS: Madison, WI, 2013.
4) O. V. Dolomanov, L. J. Bourhis, R. J. Gildea, J. A. K. Howard and H. Puschmann, OLEX2: A Complete Structure Solution, Refinement and Analysis Program, *J. Appl. Crystallogr.*, 2009, **42**, 339.
5) G. M. Sheldrick, *SHELXTL* Version 2014/7. *https://shelx.uniac.gwdg.de/SHELX/index.php.*
6) A. L. Spek, *PLATON*; The University of Utrecht: Utrecht, The Netherlands, 1999.
7) http://www.topos.ssu.samara.ru; V. A. Blatov, IUCrCompCommNewsletter 2006, 7, 4.
8) S. Nandi, D. Chakraborty and R. Vaidhyanathan, Permanently Porous Single Molecule H-Bonded Organic Framework for Selective CO_2 Capture. *Chem. Commun*., 2016, **52**, 7249-7252.
9) C. Gunathilake, J. Górka, S. Dai and M. Jaroniec, *J. Mater. Chem. A*, 2015, **3**, 11650 —11659.
10) J. Taesch, V. Heitz, F. Topić and K. Rissanen, *Chem. Commun.*, 2012, **48**, 5118-5120.
11) R. Goswami, K. Karthick, S. Das, S. Rajput, N. Seal, B. Pathak, S. Kundu and S. Neogi, *ACS Appl. Mater. Interfaces*, 2022, **14**, 29773–29787.
12) M. Horeau, G. Lautrette, B. Wicher, V. Blot, J. Lebreton, M. Pipelier, D. Dubreuil, Y. Ferrand and I. Huc, *Angew. Chem. Int. Ed.*, 2017, **56**, 6823-6827.